Electronic Supplementary Material (ESI) for Chemical Science.
This journal is © The Royal Society of Chemistry 2024

Supporting information

Restraining the shuttle effect of polyiodide and modulating the deposition of zinc ions to enhance the cycle lifespan of aqueous Zn-I_2 battery

Qu Yue,[a,*] Yu Wan,[a] Xiaoqin Li,[a] Qian Zhao,[a] Taotao Gao,[a] Guowei Deng,[b] Bing Li,[c] Dan Xiao,[a,d,*]

[a] Institute for Advanced Study, School of Mechanical Engineering, Chengdu University, Chengdu, 610106, P. R. China

[b] Sichuan Provincial Key Laboratory for Structural Optimization and Application of Functional Molecules, College of Chemistry and Life Science, Chengdu Normal University, Chengdu, 611130, P. R. China

[c] Hubei Key Laboratory of Wudang Local Chinese Medicine Research, Hubei University of Medicine, Shiyan, 442000, P. R. China

[d] College of Chemical Engineering, Sichuan University, No. 24 South Section 1, Yihuan Road, Chengdu 610065, PR China

*Corresponding authors: yuequ@cdu.edu.cn (Q. Yue), xiaodan@scu.edu.cn (D. Xiao)

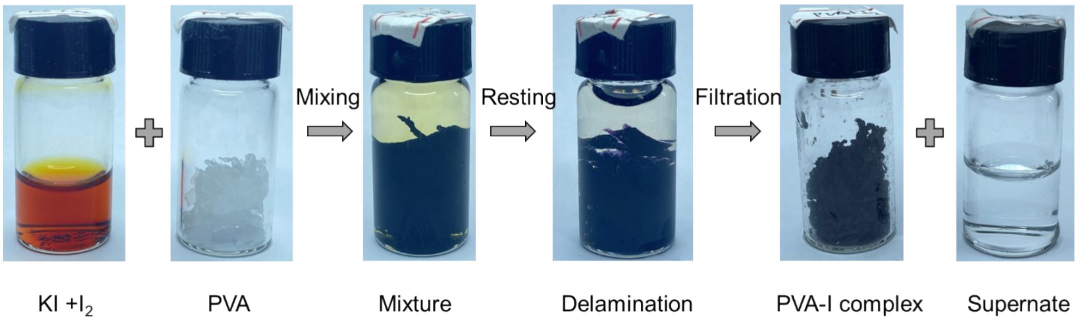

Figure S1 Photographs of the polyiodide adsorption processes by PVA.

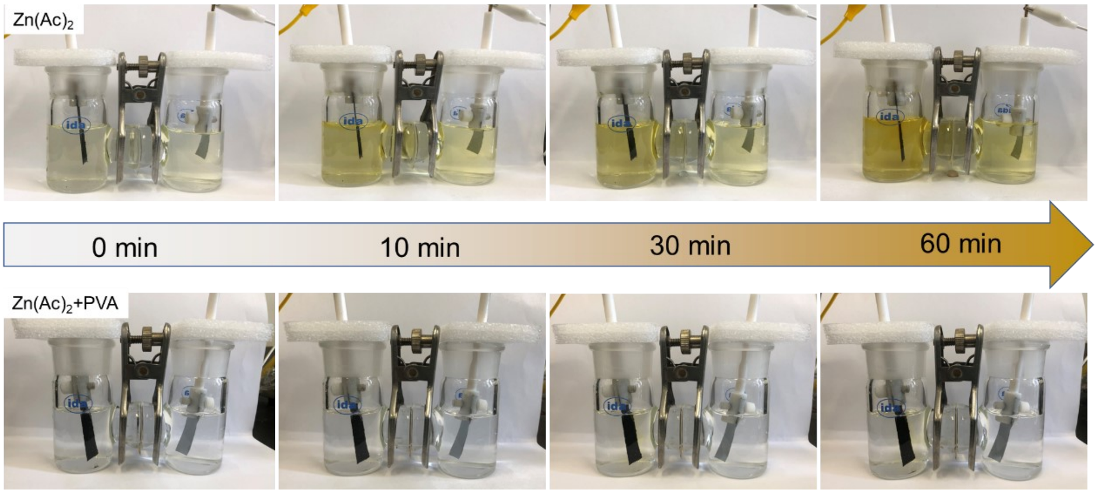

Figure S2 Visualization experiments of I_3^- shuttle effect demonstrated by H-type cell without and with PVA.

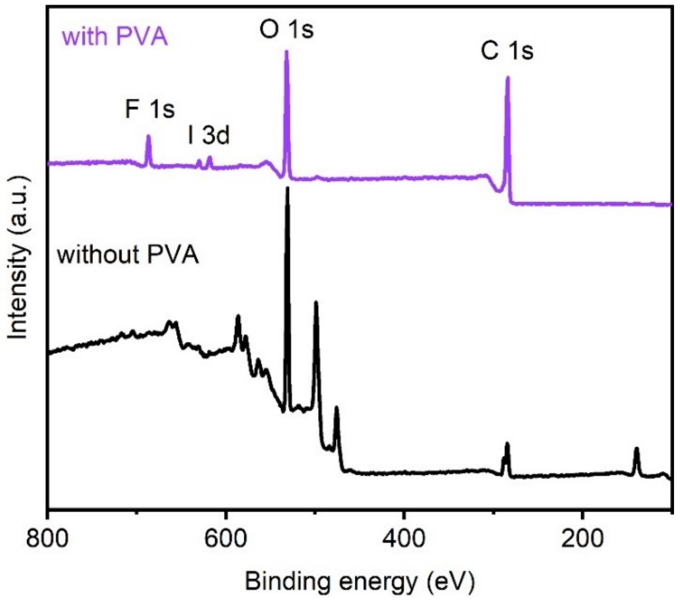

Figure S3 The full profile of the XPS spectrum.

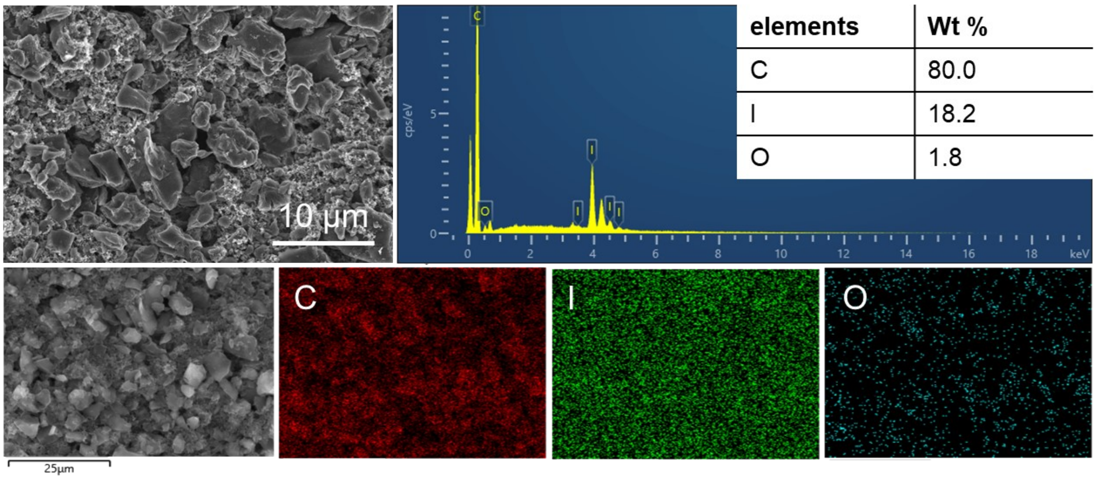

elements	Wt %
C	80.0
I	18.2
O	1.8

Figure S4 The SEM image and corresponding EDS of the cathode after cycling in PVA electrolyte.

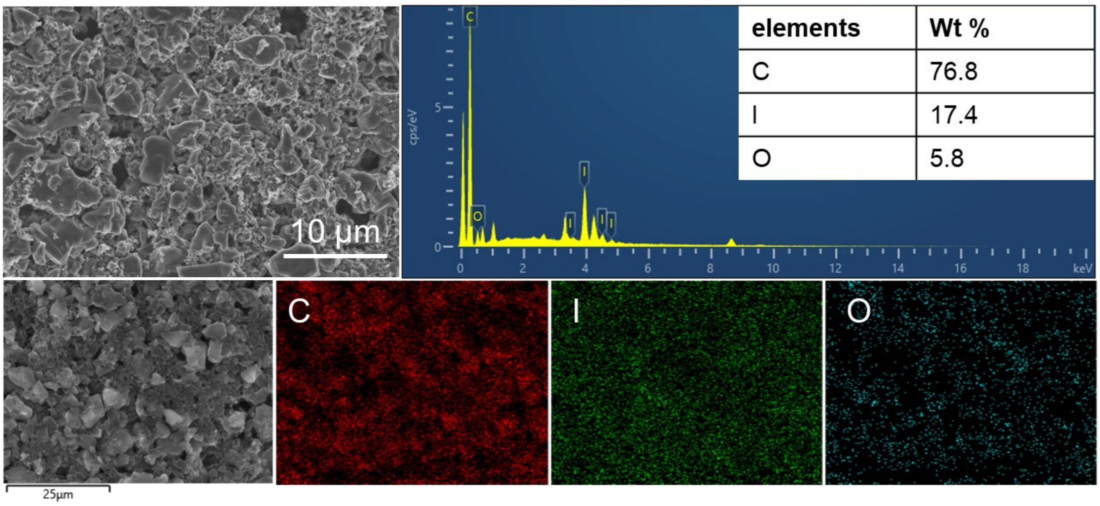

elements	Wt %
C	76.8
I	17.4
O	5.8

Figure S5 The SEM image and corresponding EDS of the cathode after cycling in PVA-free electrolyte.

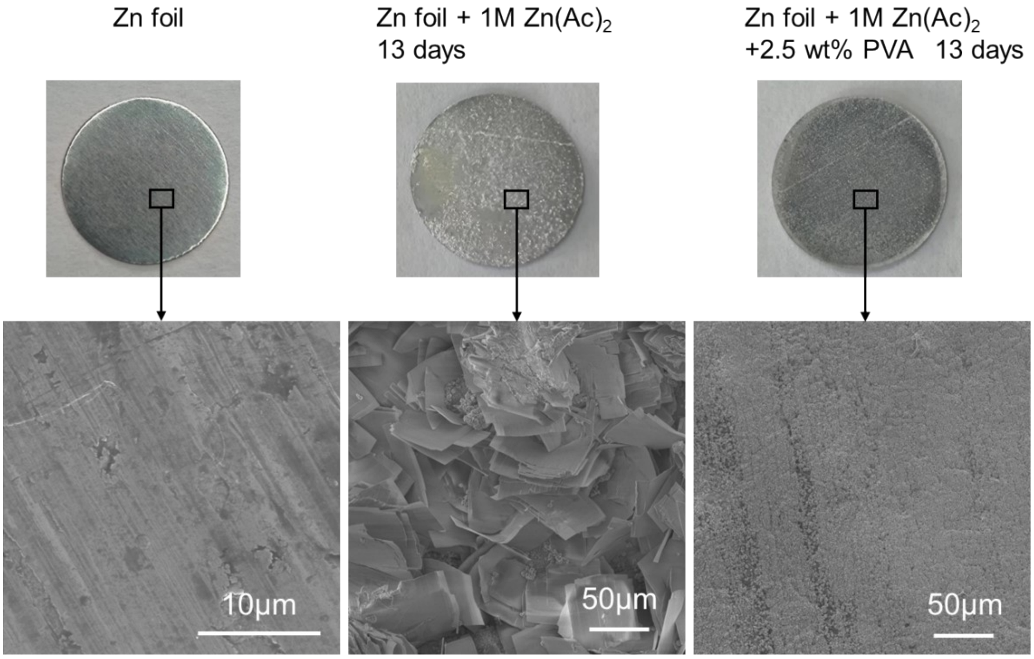

Figure S6 Optical photographs and SEM images of different Zn foils: commercial Zn foil, Zn foil immersed in $Zn(Ac)_2$ after 13 days, and Zn foil immersed in $Zn(Ac)_2$ + PVA after 13 days.

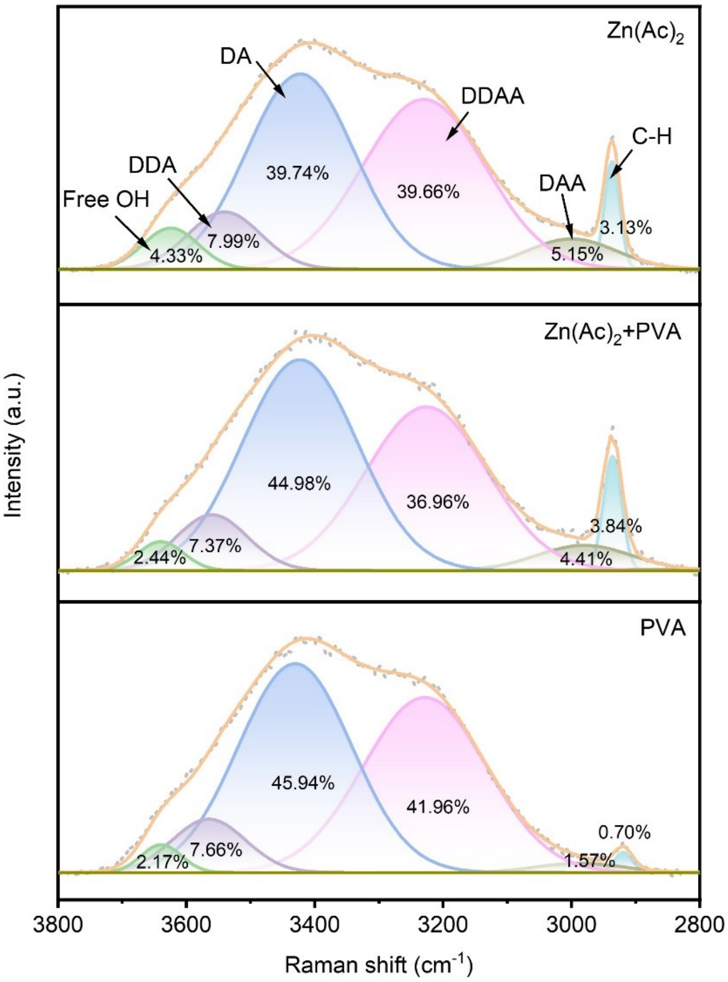

Figure S7 Raman spectra of $Zn(Ac)_2$, $Zn(Ac)_2$ + PVA, and PVA electrolyte, respectively.

On the basis of the hydrogen-bonding behavior of specific water molecules, the local hydrogen-bonded networks can be differentiated by whether the molecule forms hydrogen bonds as a proton donor (D), proton acceptor (A), or their combinations in the first shell [1]. Accordingly, the main local hydrogen-bonded networks are expected to be single donor-double acceptor (DAA), double donor-double acceptor (DDAA), single donor-single acceptor (DA), and double donor-single acceptor (DDA). At room temperature, the Raman OH stretching band of zinc acetate aqueous solution at 2800~3800 cm^{-1} can be deconvoluted into five Gaussian sub-bands, located at ~2978 cm^{-1}, ~3236 cm^{-1}, ~3405 cm^{-1}, ~3517 cm^{-1}, and ~3627 cm^{-1}, as shown in Figure S7. They are assigned to the DAA, DDAA, DA, DDA, and free OH symmetric stretching vibrations, respectively. Free OH refers to the contribution of the cation-solvated water. Figure 3h illustrates the changes in the strength of the five Gaussian sub-bands when the PVA additive is added to the solution. The decreased proportion of DAA and free OH means less active water molecules [2].

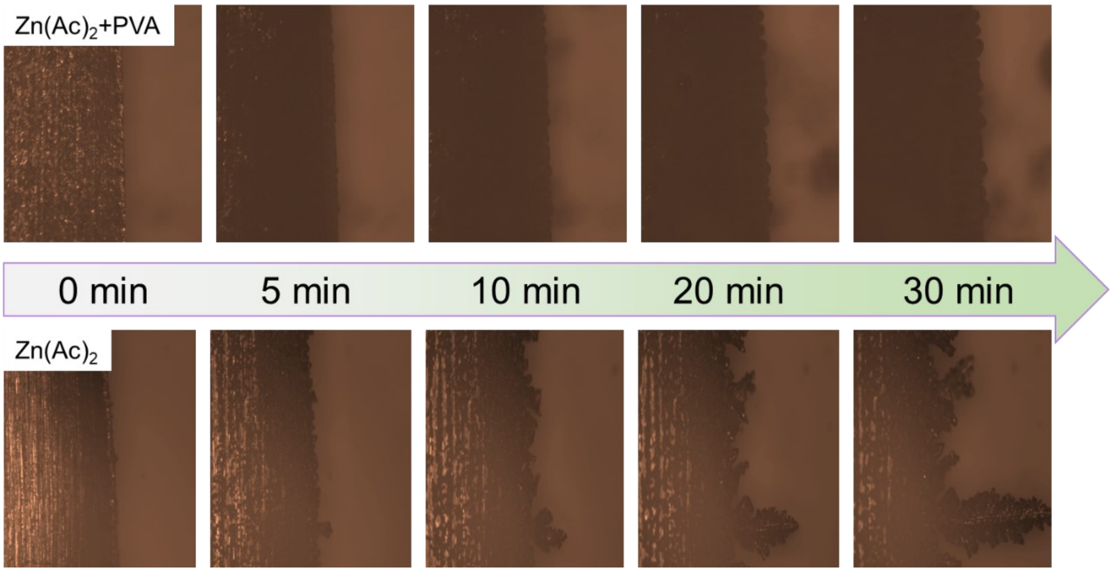

Figure S8 In situ optical photographs of Zn deposition onto Zn foil with and without PVA.

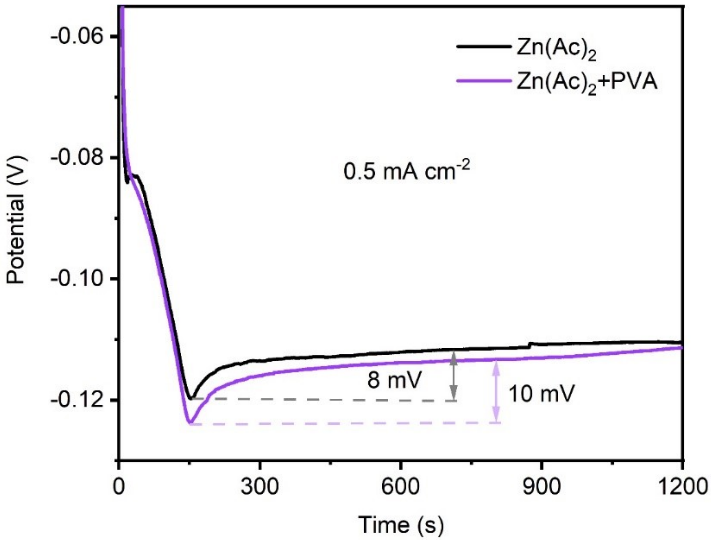

Figure S9 Voltage-time profiles of nucleation on Zn||Cu batteries overpotential at 0.5 mA cm^{-2}.

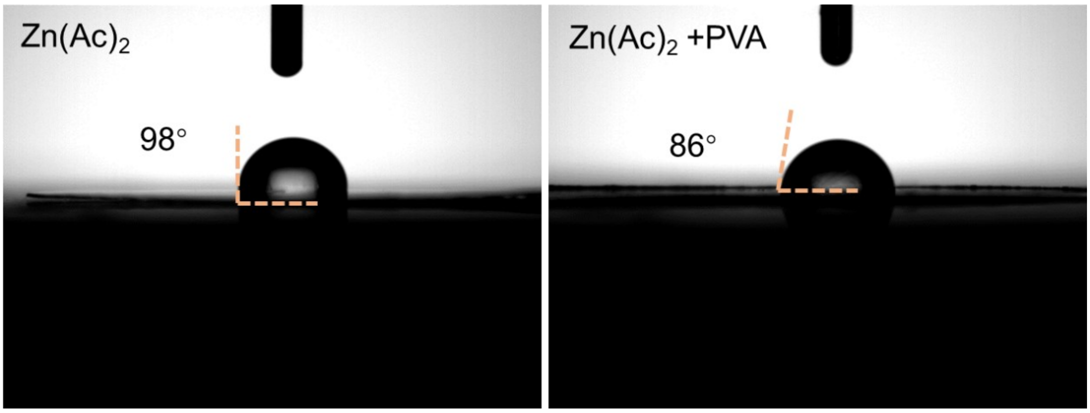

Figure S10 The contact angle values of Zn metal electrode with respect to the electrolytes with and without PVA.

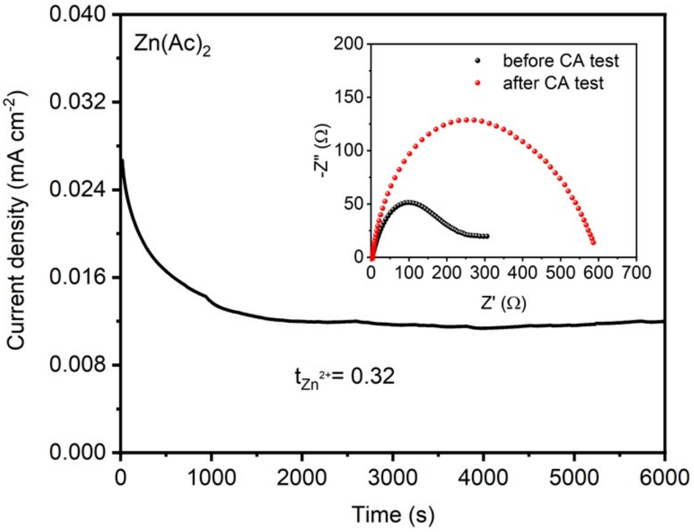

Figure S11 The CA curve of Zn||Zn battery (the inset show corresponding Nyquist plots at the initial and steady states).

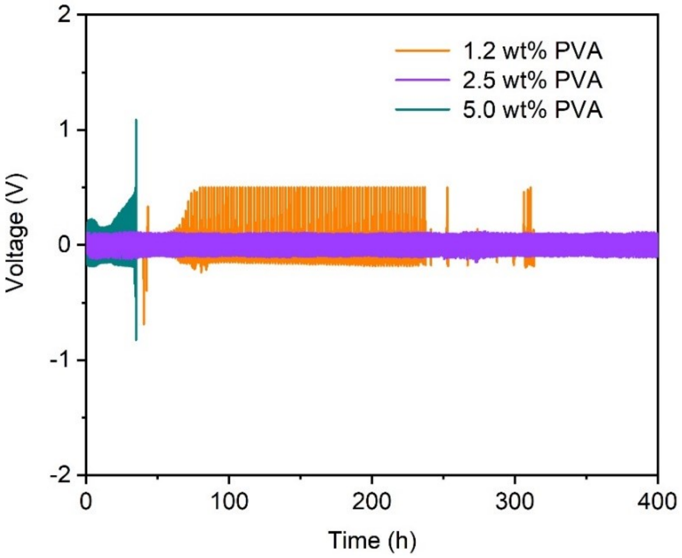

Figure S12 The cycling performances of Zn||Zn batteries with different content of PVA under 1 mA cm^{-2} and 1 mAh cm^{-2}.

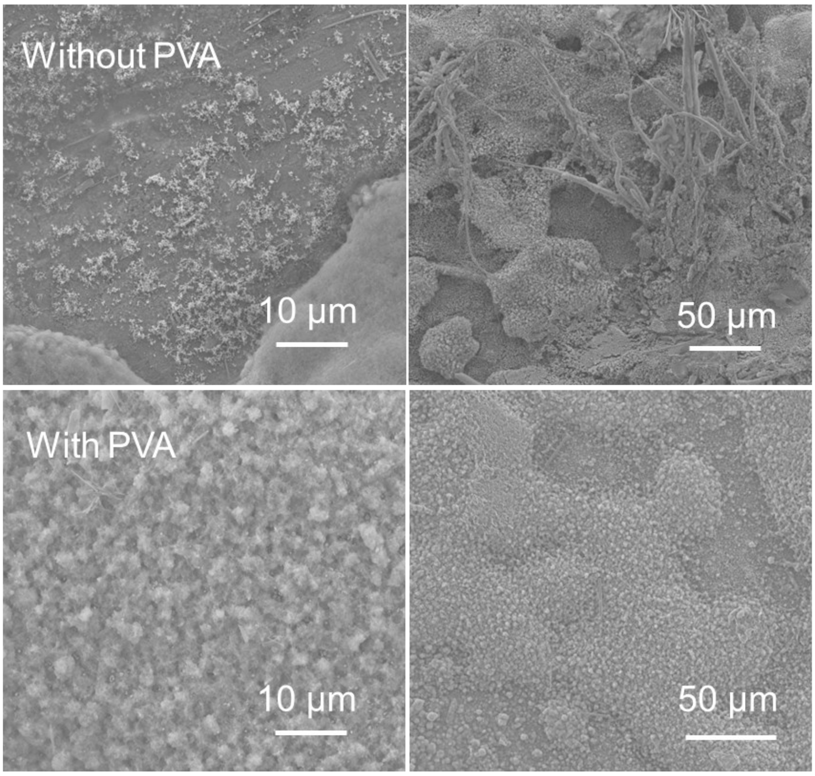

Figure S13 SEM of the Zn anode surface using Zn||Zn batteries with and without PVA after Zn plating and stripping for 20 cycles at a current density of 2.0 mA cm^{-2}.

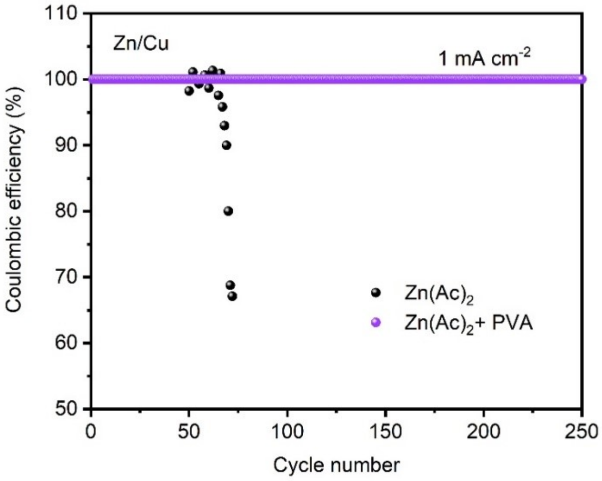

Figure S14 The CE of Zn||Cu batteries with and without PVA.

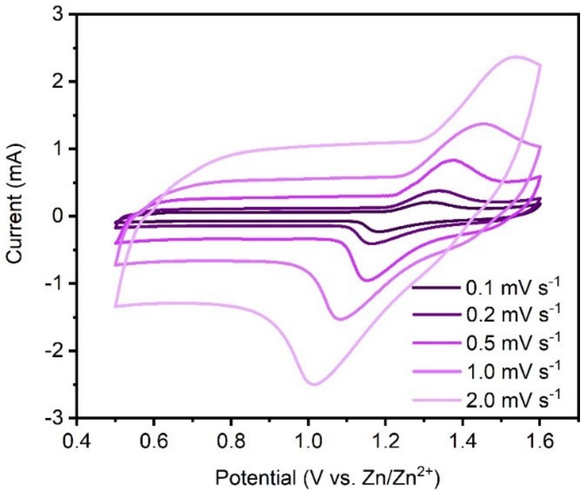

Figure S15 CV curves of the Zn-I_2 battery with PVA at different scan rates from 0.1 mV s^{-1} to 2.0 mV s^{-1}.

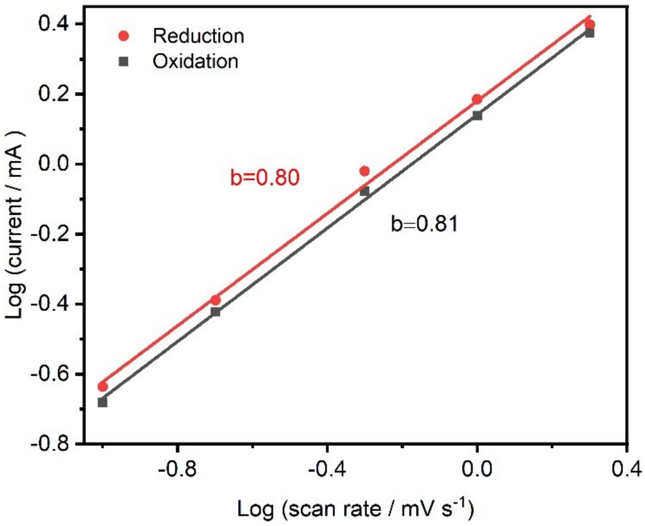

Figure S16 The plots of log (i) vs log (ν), data was collected from CV curves.

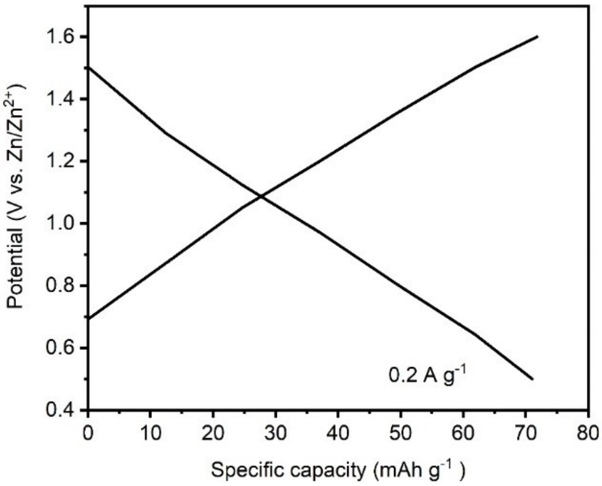

Figure S17 The capacitance contribution of the porous carbon electrode.

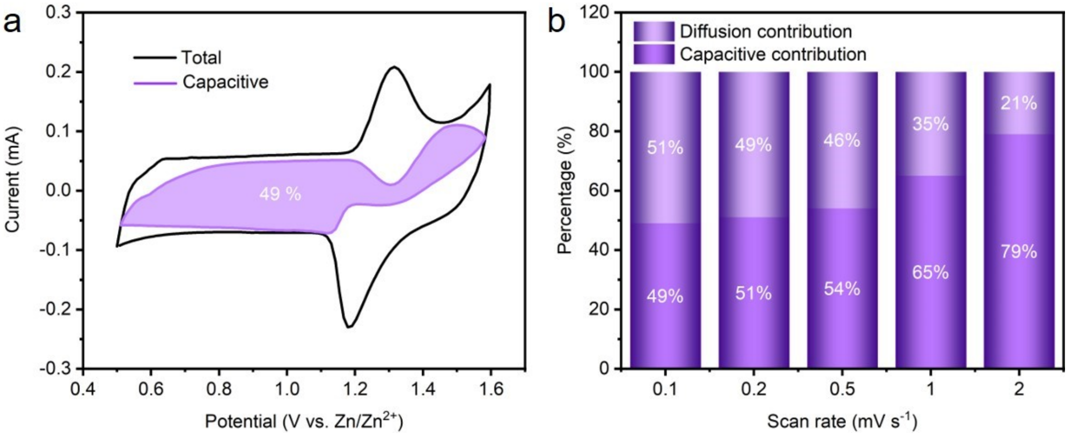

Figure S18 (a) The capacitive contributions of the battery at a sweep rate of 0.1 mV s^{-1}. (b) the capacitive contributions of the battery at sweep rates of 0.1, 0.2, 0.5, 1.0, and 2.0 mV s^{-1}.

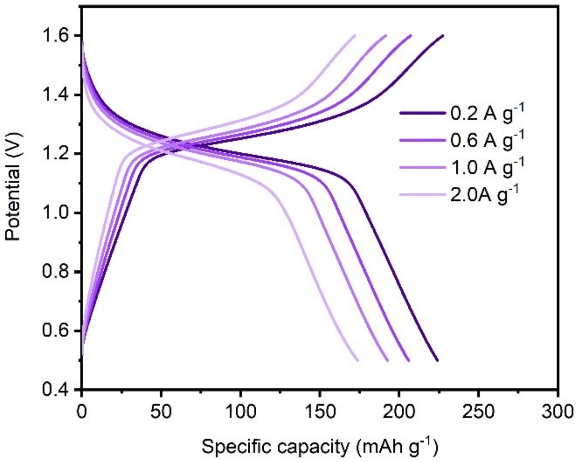

Figure S19 Galvanostatic charge-discharge profile of the Zn-I_2 battery without PVA at different current densities.

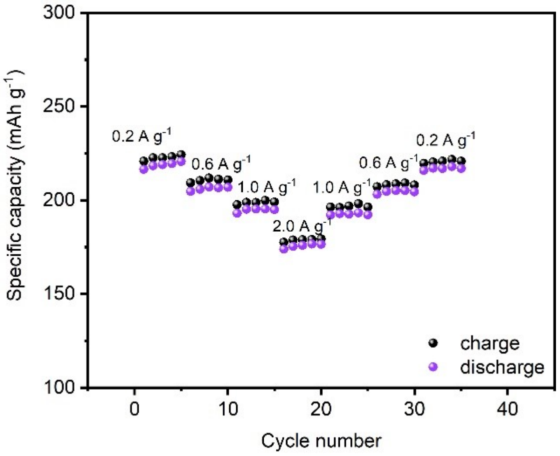

Figure S20 The rate performance of the Zn-I_2 battery without PVA at different current densities.

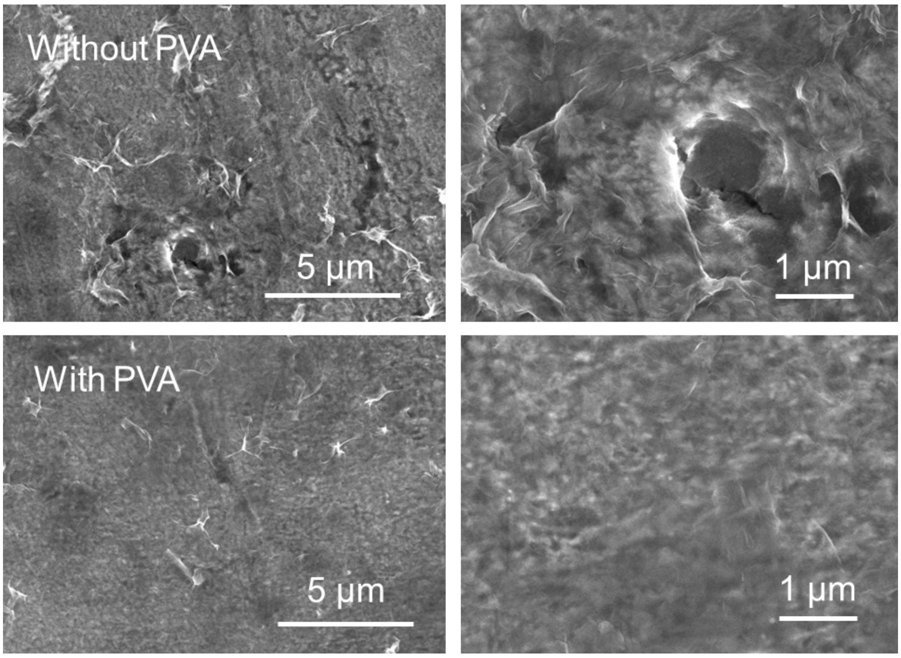

Figure 21 SEM images of Zn foils after charging and discharging 20 cycles of the Zn-I_2 full battery with/without PVA additive.

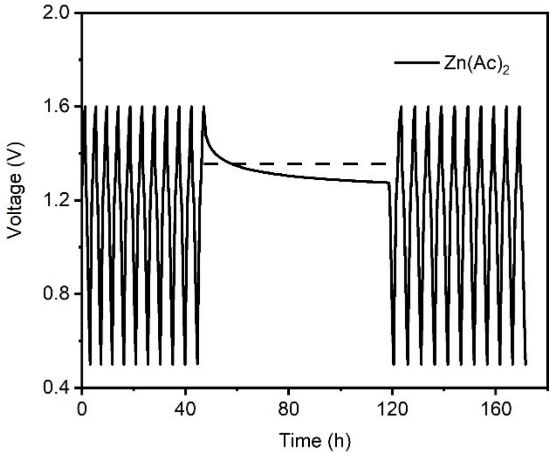

Figure S22 Self-discharge characteristics for Zn-I_2 batteries without PVA.

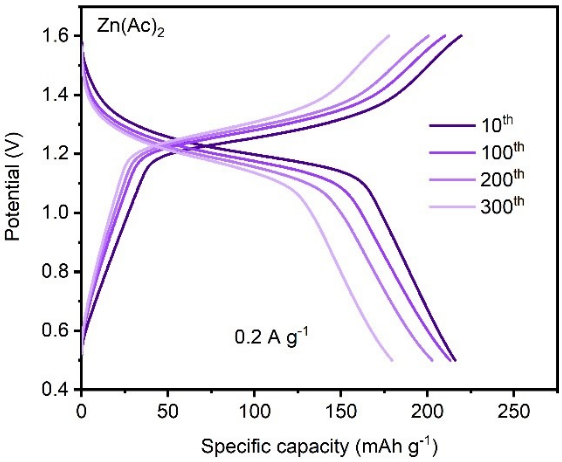

Figure S23 Galvanostatic charge/discharge profiles of different cycles at 0.2 A g^{-1} in the Zn-I_2 battery without PVA.

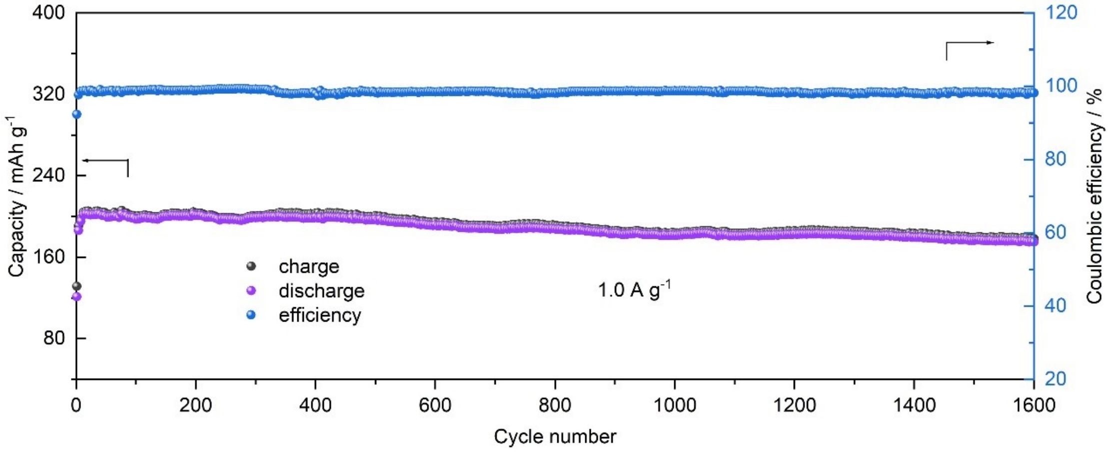

Figure S24 Long-term cycling performance of the Zn-I_2 battery with PVA at 1.0 A g^{-1}.

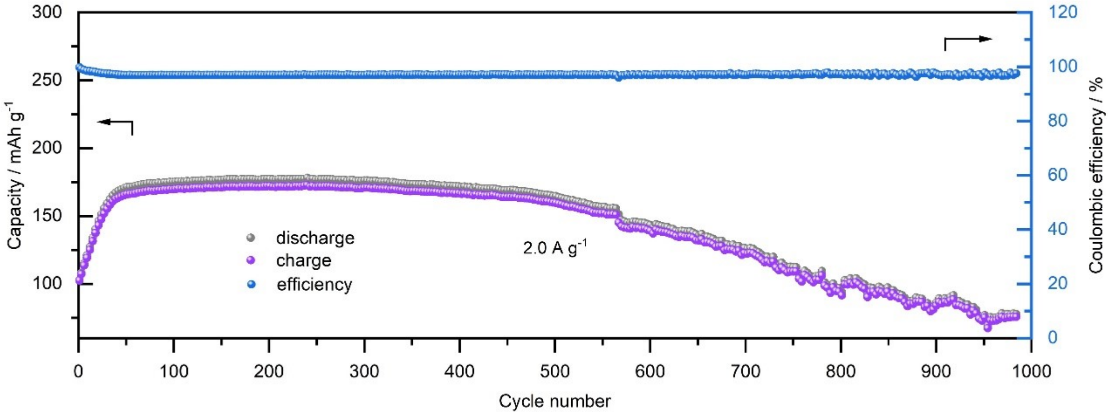

Figure S25 Long-term cycling performance of the Zn-I_2 battery without PVA at 2.0 A g^{-1}.

References

[1] Q. Sun, A Local Statistical Structural Model for Amorphous Solids, Chinese Physics Letters, 30 (2013) 126102.

[2] H. Yang, D. Chen, R. Zhao, G. Li, H. Xu, L. Li, X. Liu, G. Li, D. Chao, W. Han, Reunderstanding aqueous Zn electrochemistry from interfacial specific adsorption of solvation structures, Energy & Environmental Science, 16 (2023) 2910-2923.